Suspensions of rod-like colloids and a depleting agent under confinement

2008 J. Phys.: Condens. Matter 20 404223

(http://iopscience.iop.org/0953-8984/20/40/404223)

IOP PUBLISHING JOURNAL OF PHYSICS: CONDENSED MATTER
J. Phys.: Condens. Matter **20** (2008) 404223 (6pp) doi:10.1088/0953-8984/20/40/404223

Suspensions of rod-like colloids and a depleting agent under confinement

S Jungblut, K Binder and T Schilling

Institut für Physik, Johannes Gutenberg-Universität, D-55099 Mainz, Staudinger Weg 7, Germany

Received 28 March 2008
Published 10 September 2008
Online at stacks.iop.org/JPhysCM/20/404223

Abstract
We present a computer simulation study of suspensions of rod-like colloids and a depletant in confinement to a slit-pore. Mixtures of hard spherocylinders and ideal spheres were studied by means of Monte Carlo simulations in the grand canonical ensemble. By use of finite size scaling analysis we determined the critical behaviour. In order to overcome large barriers in the free energy we applied the successive umbrella sampling method (Virnau and Müller 2004 *J. Chem. Phys.* **120** 10925). We find that, under confinement, the critical point of gas–liquid demixing shifts to higher concentrations of rods and smaller concentrations of spheres due to the formation of an orientationally ordered surface film. If the separation between the walls becomes very small, the critical point is shifted back to smaller concentrations of rods because the surface film breaks up. In particular, we present a method for determining the wetting behaviour from an analysis of the distribution of particle concentration. For large wall separations we find wetting near the critical point consistent with the Cahn argument.

1. Introduction

The reason for our interest in mixtures of rod-like colloids and depletants is twofold. From the experimental point of view, such mixtures are relevant in various fields of physics: suspensions of viruses and polymers have been successfully studied as a colloidal model system for liquid crystals for several years [1, 2]. Recently, such suspensions have in particular been used to study non-equilibrium effects [3–5]. Mixtures of carbon nanotubes and micelles suspended in a polymeric matrix are an interesting candidate for low-weight conducting material use (see [6] and references therein). And even the assembly of the cytoskeleton (being a structure composed of rod-like objects in a very crowded environment) has been discussed in the framework of a rod-plus-depletant model [7].

As regards theoretical statistical mechanics, rod–sphere mixtures under confinement offer insight into surface induced ordering phenomena. In the bulk, such mixtures exhibit gas–liquid coexistence with a critical point of the Ising universality class (as long as the aspect ratio of the rods is sufficiently small) [8]. However, in confinement, orientational order is induced by the walls. This order affects the phase transitions and the critical behaviour of the system. Understanding these effects is interesting from the point of view of critical phenomena, as well as a prerequisite for applications of liquid crystals in microfluidic devices.

Several related issues have recently been addressed by other groups. Dijkstra, van Roij and Evans studied suspensions of hard rods in confinement between hard walls close to the isotropic–nematic transition in Gibbs ensemble simulations [9] and within the Zwanzig model [10, 11]. They found that a uniaxial surface phase forms at low concentrations. At higher concentrations the surface film undergoes a transition to biaxial order, and on further approach of the isotropic–nematic transition, its thickness diverges.

Rods in two dimensions—i.e. the limiting case of an infinitely thin confining slit-pore—have been studied with emphasis on several aspects of orientational order [12–16].

Sphere–sphere mixtures in confinement have been simulated by Gibbs ensemble Monte Carlo methods [17] and with the successive umbrella sampling method [18–21]. In particular, in the studies by Vink and co-workers the crossover from 3D to 2D critical behaviour was investigated.

Here, we present a study of mixtures of hard rods and freely interpenetrable spheres (i.e. an extension of the Asakura–Oosawa model [22, 23] to include orientational degrees of freedom), which were confined to hard-walled slit-pores. By means of Monte Carlo simulation in the grand canonical ensemble and by finite size scaling analysis, we have determined the phase boundaries of isotropic–isotropic coexistence in the bulk and in confinement. In particular, we present a method by which the contact angle of a droplet in contact with a wall can be determined from simulations in the grand canonical ensemble. We discuss the wetting properties of the rod–sphere system.

2. Model and simulation method

The rod-like colloidal particles were modelled as hard spherocylinders of length L and diameter D. The spherical depletants were of the same diameter. They were freely interpenetrable among each other and hard with respect to the rods. Hence, this model is an extension of the Asakura–Oosawa model to rod-like colloids. The Monte Carlo simulations were performed in the grand canonical ensemble, where the chemical potentials $\mu_{r/s}$ of rods and spheres, the volume V of the simulation box and the temperature T were fixed. The numbers of rods N_r and spheres N_s were allowed to fluctuate, which was realized by insertions and removals of particles. Minimal image periodic boundary conditions were applied in the dimensions parallel to the walls. The interactions of rods and spheres with the walls were modelled to be hard. The system was equilibrated with the usual insertion/removal moves of spherocylinders and spheres as well as with a grand canonical cluster move, which considerably improves the acceptance probability, especially in the sphere-dense phase [8].

The energetically unfavourable states were explored with help of the successive umbrella sampling method [24]. Probabilities of finding a specific volume fraction of rods (defined as $\eta_r = N_r v_r / V$ with $v_r = \pi D^3(2+3L/D)/12$, the volume of a spherocylinder) at given sphere fugacity $z_s = \exp(\mu_s/k_B T)$ were sampled in the simulations. The chemical potential of spheres plays the role of an inverse temperature for the attractive forces arising between the rods due to the presence of the depletant.

The results of a simulation for a given chemical potential of rods μ_r^{sim} can be rescaled to any chemical potential μ_r via

$$\ln[P_{\mu_r}(N_r)] = \ln[P_{\mu_r^{\mathrm{sim}}}(N_r)] + (\mu_r - \mu_r^{\mathrm{sim}})N_r. \qquad (1)$$

The clue in this observation is that the coexistence distribution can be obtained from simulations at any chemical potential. At coexistence, the distribution $P_{\mu_r}(N_r)$ is bimodal, i.e. the areas under the two peaks are equal [25]. The mean values of the peak positions are the volume fractions of the coexisting states.

The position of the critical point is derived from the crossing point of the cumulant ratios [25, 26], defined as $U_4 = \langle m^4\rangle/\langle m^2\rangle^2$ with $m = \eta_r - \langle\eta_r\rangle$, as a function of sphere fugacity for different system sizes. The systems considered were rectangular $L_\parallel \times L_\parallel \times d$ boxes, with $L_\parallel$ chosen in the range from d to $d + 3L$ with periodic boundary conditions in the directions parallel to the confining walls. The rod volume fraction which corresponds to the critical sphere fugacity is approximated as the average of the volume fractions of the coexisting rod-rich and rod-poor phases $\eta_r^c = (\eta_r^l + \eta_r^g)/2$. Typically, 3×10^7 Monte Carlo insertion/removal moves were attempted per sampling window in successive umbrella sampling simulations. For each volume fraction of rods, the volume fraction of spheres present in the system was measured and averaged over the number of times that this rod volume fraction occurred. The critical sphere volume fraction is the one which corresponds to the critical rod volume fraction and was measured at the critical sphere fugacity. The position of the critical point was derived after simulating the system; thus, the value of the critical sphere fugacity was not known beforehand. If no simulation runs were available at the critical sphere fugacity, the sphere volume fractions from the results of the simulations with closest larger and smaller values of the fugacity were used to limit the range in which the required critical sphere volume fraction lies.

In order to study the orientational ordering effects, we measure profiles of the nematic order parameter S, which is defined as the absolute largest eigenvalue [27] of the tensor

$$\mathbf{Q}(z) = \frac{1}{2\tilde{N}_r}\sum_{i=0}^{\tilde{N}_r}\left(3\mathbf{u}^i \cdot \mathbf{u}^i - \mathbf{I}\right) \qquad (2)$$

where $\mathbf{u}^i$ is the unit vector in the direction of the orientation of the rod i and $\mathbf{I}$ is the identity matrix. The space between the walls is divided into thin slices, so $\tilde{N}_r$ is the number of rods in such a slice at the distance z/D from the middle of the simulation box.

S indicates whether there is a preferred direction in the system and how strongly the rods are oriented with respect to it. The eigenvector to this eigenvalue is called the director. If S is zero, the phase is completely isotropic. If S is unity, all rods are aligned parallel to the director (nematic order). If S is negative, they lie perpendicular to the director (commonly called 'uniaxial order', although the nematic phase is uniaxial, too). The biaxiality measure ξ is half of the difference of the other two eigenvalues of the matrix $\mathbf{Q}$. It shows whether there is another preferred direction in the plane perpendicular to the director.

3. Results

3.1. Phase diagram

Figure 1 shows the phase diagram that we obtained for rods of aspect ratio $L/D = 3$ at wall separations $d = 3, 6, 9, 15\ D$ and in the bulk. The phase boundaries are indicated. The smaller the distance between the walls, the larger the sphere fugacity which is required for demixing.

Table 1 sums up the positions of the critical point for various wall distances. When the system is confined, the critical point lies at a higher rod volume fraction than in the bulk. However, once in confinement, the shifts in the critical rod volume fraction in comparison to the bulk are almost the same for all wall separations, as long as the distance between the walls is large enough for the correlations, which are induced by the walls, to decay before the centre of the pore is reached.

To study structural changes due to the interaction of the rods with the walls, the gas-like and liquid-like phases were simulated under confinement in the canonical ensemble (fixed number of spherocylinders N_r, spheres N_s as well as the volume of the simulation box). The number of particles

Table 1. Critical point in confinement.

d/D	$z^{c}_{s,conf}$	$\eta^{c}_{r,conf}$	$\eta^{c}_{s,conf}$	$\mu^{c}_{r,conf}$
3	1.85 ± 0.03	0.157 ± 0.002	0.30 ± 0.01	10.1 ± 0.2
4	1.59 ± 0.02	0.164 ± 0.002	0.29 ± 0.01	8.9 ± 0.1
5	1.48 ± 0.02	0.169 ± 0.002	0.27 ± 0.01	8.5 ± 0.1
6	1.38 ± 0.02	0.169 ± 0.002	0.26 ± 0.01	8.0 ± 0.1
9	1.26 ± 0.01	0.169 ± 0.002	0.25 ± 0.01	7.35 ± 0.05
12	1.22 ± 0.01	0.169 ± 0.002	0.25 ± 0.01	7.04 ± 0.05
15	1.18 ± 0.01	0.166 ± 0.002	0.25 ± 0.01	6.74 ± 0.05
∞	1.109 ± 0.001	0.131 ± 0.002	0.30 ± 0.01	6.208 ± 0.005

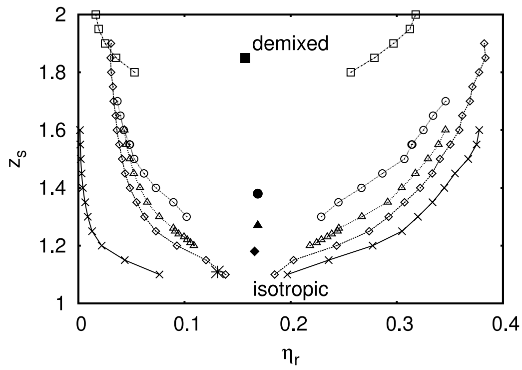

Figure 1. Phase diagram for a mixture of spherocylinders with aspect ratio $L/D = 3$ and spheres of diameter D in bulk (crosses) and between two hard walls at distances $d = 3\ D$ (squares), 6 D (circles), 9 D (triangles) and 15 D (diamonds). The filled symbols mark the critical points. Curves are guides to the eye only, connecting data for the rod volume fractions of the coexisting phases rich (right) and poor (left) in rods, for systems of lateral linear dimensions $L_{\parallel} = 12\ D$ for $d = 6, 9\ D$ and $L_{\parallel} = 18\ D$ for $d = 3, 15\ D$.

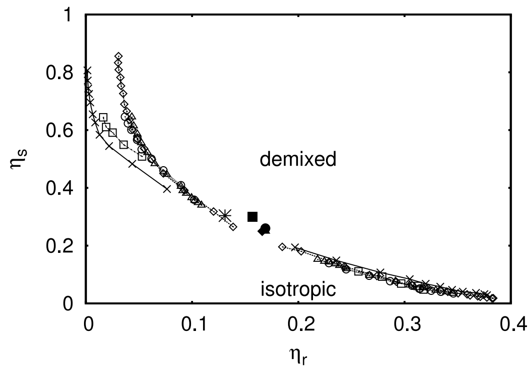

Figure 2. Phase diagram of figure 1 in the (η_r, η_s) plane.

was chosen to match the coexistence values determined in the grand canonical ensemble. Although in principle the finite size effects are different in the canonical and grand canonical ensembles [25], far enough from the critical point this difference can safely be neglected.

Figure 3 shows profiles of the nematic order parameter (bottom) and of the rod volume fraction changes in the gas-like and liquid-like phases due to the walls. The biaxiality parameter ξ (not shown here) fluctuates around zero in both phases. The nematic order parameter of the gas-like phase in the middle of the box is not shown here, since the number of rods from which this parameter has to be calculated is very small and the statistics were extremely poor. Although longer simulation runs and larger system sizes would yield a better estimate for the nematic order parameter, the effort is redundant, since a simple look at the snapshots provides convincing evidence that the phase considered is an isotropic gas. In the more important area close to the walls the sampling of the nematic order parameter works well, since the number of rods is sufficient for getting reliable results.

The hard walls induce a layered uniaxial phase (see the sketch in figure 4), whose thickness is of the order of the rod length. The phases between these two uniaxial films have the same properties as the usual bulk gas-like and liquid-like phases. Hence, confinement shifts the phase diagram in terms of the rod volume fraction such that the uniaxial layered films are introduced to the system. The gas-like phase is moved to larger rod volume fractions since the density of the uniaxial film is larger than it is in the bulk gas-like phase. The density of the uniaxial film in the liquid-like phase is smaller than in the bulk due to the layering effects as can be seen in figure 3, upper panel. Thus, the liquid-like branch is shifted to smaller volume fractions. As long as the uniaxial layers on the walls do not interact, these changes do not depend on the distance between the walls. Once the layers start to interact—roughly at $d < 2L$—the separation distance d becomes important. Gas–liquid demixing then occurs laterally inside the layers.

In terms of the sphere fugacities, the phase diagram is continuously shifted to higher values. However, if one considers the actual volume fraction of spheres in the mixture instead of their chemical potential, the phase diagram remains almost unchanged by confinement, as indicated in figure 2, provided the demixing transition occurs in the bulk-like central region and not in the uniaxial layers at the walls. The shift in the fugacities is due to the reduced volume available between the uniaxial films. At decreasing wall separation the free volume accessible to spheres between the uniaxial layers of rods becomes smaller; therefore the chemical potential needed to keep the spheres in equilibrium with the rods increases. The sphere volume fraction in the system stays constant as long as the rod volume fraction of the stable phase does not change due to moving the walls.

3.2. Wetting behaviour

From the successive umbrella sampling simulations a profile $P(\eta_r)$ is obtained. Its logarithm corresponds (up to a constant) to the effective free energy as a functional of the rod volume

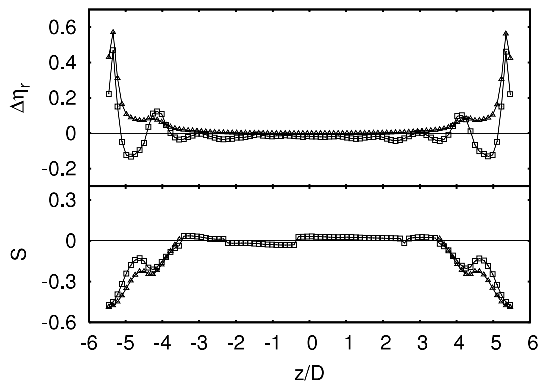

Figure 3. Confinement induced difference in volume fraction of the rods $\Delta\eta_r = \eta_r^{conf} - \eta_r^{bulk}$ for the gas-like (open triangles) and liquid-like (open squares) phases (top). Nematic order parameter S in the gas-like (open triangles) phase at the walls and in liquid-like (open squares) phase (bottom). The distance between the walls is $d = 12\,D$; the rod aspect ratio $L/D = 3$. The corresponding sphere fugacity is $z_s = 1.4$. These data refer to a lateral linear dimension $L_\parallel = 24\,D$.

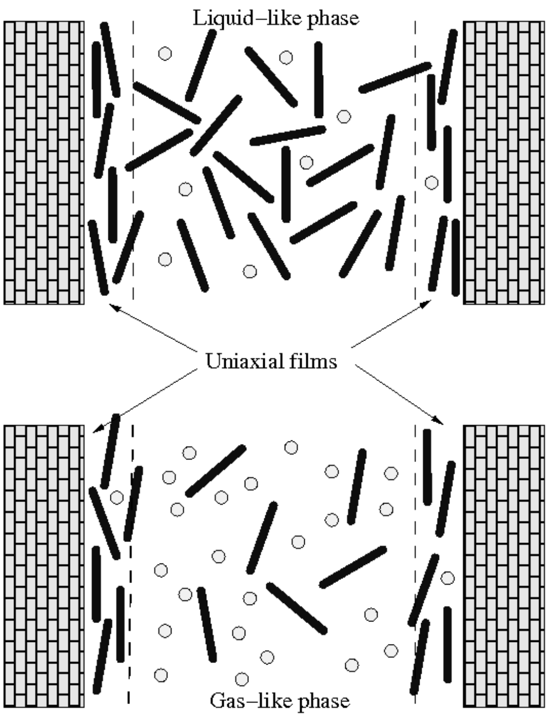

Figure 4. Sketches of configurations in confinement. Close to the walls, the system forms a uniaxial film; further away it behaves as in the bulk liquid (upper panel) or bulk gas (lower panel).

fraction. Thus, the differences in free energy of various states can be extracted from this profile. Consider the gas-like phase. The rod volume fraction which would be stable in the bulk at a fixed sphere fugacity is known from previous simulations [8].

Now, the free energy difference between this value and the value of the gas-like phase stable in confinement, ΔF_1, can be read off the free energy profile, as indicated in figure 5. This difference is the free energy needed to create the interfaces of the bulk-like gas phase (g) with the walls (w). The

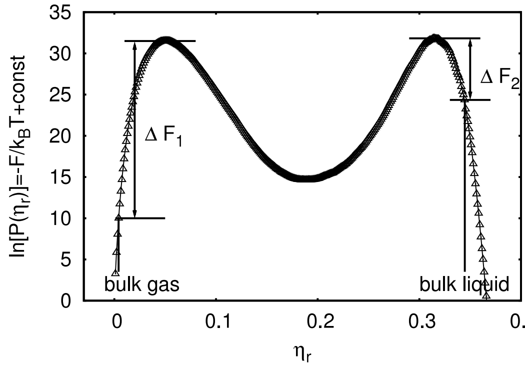

Figure 5. Free energy $\ln[P(\eta_r)]$ for spherocylinders between the walls at distance $d = 12\,D$ and sphere fugacity $z_s = 1.4$. ΔF_1 and ΔF_2 indicate the energy differences between the states stable in the bulk and in confinement on the gas-like and on the liquid-like sites on the phase diagram.

corresponding interfacial tension $\gamma_{g,w}$ can be calculated as

$$\gamma_{g,w} = \frac{\Delta F_1}{2A} \tag{3}$$

with A the area of one wall. Similarly, the tension of the interface between the liquid-like phase (l) and the wall can be determined:

$$\gamma_{l,w} = \frac{\Delta F_2}{2A} \tag{4}$$

with ΔF_2 the free energy difference between the liquid-like branches in the rod volume fraction in bulk and in confinement.

Assume that the liquid-like phase forms a droplet on the wall. According to Young's law, the contact angle $\theta_{g,l}$ is determined by

$$\gamma_{g,l}\cos\theta_{g,l} = \gamma_{g,w} - \gamma_{l,w}. \tag{5}$$

The tension of the interface between the gas-like and the liquid-like phases was calculated in the previous simulations [8]; the interfacial tension difference on the right-hand site of the equation can be obtained by subtracting equation (4) from (3). Thus, everything needed to determine the contact angle is known.

Figure 6 shows the cosine of the contact angle obtained in this way at wall separations $d = 9, 12, 15\,D$. On approach to the critical point the ratio $(\gamma_{g,w} - \gamma_{l,w})/\gamma_{g,l}$ is expected to show power law behaviour [28] with the exponent $\beta_1 - \mu \approx -0.5$, where $\beta_1 \approx 0.8$ is the surface critical exponent [29–31] and $\mu \approx 1.3$ is the gas–liquid interfacial tension exponent. Lines in figure 6 indicate the predicted power law. Since $\cos\theta_{g,l}$ cannot exceed unity, the point where this ratio reaches unity determines the value of z_s at which (for $d \to \infty$) the wetting transition occurs.

4. Discussion and summary

We have presented computer simulation studies of suspensions of rods and depleting spheres under confinement to a slit-pore. In confinement, the critical point is shifted to higher volume fractions of rods as compared to the bulk, because uniaxially

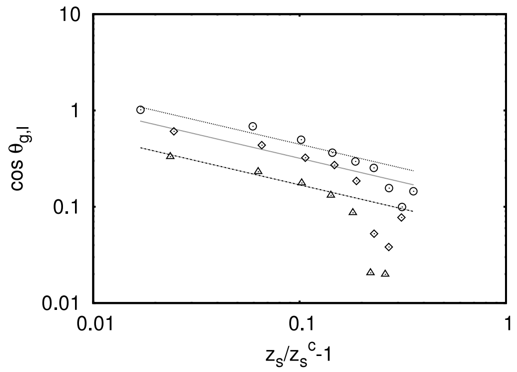

Figure 6. $\cos\theta_{g,l}$ as a function of the distance from the critical point for wall separations $d = 9\ D$ (squares), $12\ D$ (diamonds) and $15\ D$ (circles). The slope of the lines is -0.5 (they are not fitted).

ordered surface layers form close to the walls. Unless the wall separation is reduced to less than twice the uniaxial film thickness, the critical volume fraction of rods stays almost constant on decrease of the distance between the walls. Once the uniaxial layers at the walls start to interact, the critical point is shifted back in the direction of the bulk critical rod volume fraction.

We have introduced a method by which the wetting behaviour can be extracted from the grand canonical distribution of particle concentration. On approach to the critical point, the system shows complete wetting in accordance with the Cahn argument. Contact angles of droplets in the regime of incomplete wetting are estimated without the need for simulating such wall-attached large droplets.

Experimentally, suspensions of rods and depletant are relevant in various contexts, such as colloidal liquid crystal models made from fd-virus and polymers, low-weight conductors made from carbon nanotubes and surfactant micelles, and actin filaments in the crowded environment of the cell. Therefore we hope that our calculations can serve as a guideline to what can be expected in experiments if the systems are confined to a slit-pore.

Acknowledgments

We would like to thank Jürgen Horbach, Richard Vink and Peter Virnau for helpful suggestions. This work was part of the priority programme SFB Tr6 (project D5) of the German Research Association (DFG). It was partially funded by the DFG Emmy-Noether-Programme, the MWFZ Mainz and the EU network of excellence SOFTCOMP. We thank the Forschungszentrum Jülich for CPU time on the JUMP.

References

[1] Dogic Z and Fraden S 2006 Ordered phases of filamentous viruses *Curr. Opin. Colloid Interface Sci.* **11** 47
[2] Dogic Z, Prudy K R, Grelet E, Adams M and Fraden S 2004 Isotropic–nematic phase transition in suspensions of filamentous virus and the neutral polymer dextran *Phys. Rev.* E **69** 051702
[3] Dhont J K G, Lettinga M P, Dogic Z, Lenstra T A J, Wang H, Rathgeber S, Carletto P, Willner L, Frielinghaus H and Lindner P 2003 Shear-banding and microstructure of colloids in shear flow *Faraday Discuss.* **123** 157
[4] Kang K G, Lettinga M P, Dogic Z and Dhont J K G 2006 Vorticity banding in rodlike virus suspensions *Phys. Rev.* E **74** 026307
[5] Lettinga M P and Dhont J K G 2004 Non-equilibrium phase behaviour of rod-like viruses under shear flow *J. Phys.: Condens. Matter* **16** S3929
[6] Vigolo B, Coulon C, Maugey M, Zakri C and Poulin P 2005 An experimental approach to the percolation of sticky nanotubes *Science* **309** 920
[7] Borukhov I, Bruinsma R F, Gelbart W M and Liu A J 2005 Structural polymorphism of the cytoskeleton: a model of linker-assisted filament aggregation *Proc. Natl Acad. Sci. USA* **102** 3673
[8] Jungblut S, Tuinier R, Binder K and Schilling T 2007 Depletion induced isotropic–isotropic phase separation in suspensions of rod-like colloids *J. Chem. Phys.* **127** 244909
[9] Dijkstra M, van Roij R and Evans R 2001 Wetting and capillary nematization of a hard-rod fluid: a simulation study *Phys. Rev.* E **63** 051703
[10] van Roij R, Dijkstra M and Evans R 2000 Orientational wetting and capillary nematization of hard-rod fluids *Europhys. Lett.* **49** 350
[11] van Roij R, Dijkstra M and Evans R 2000 Interfaces, wetting, and capillary nematization of a hard-rod fluid: theory for the Zwanzig model *J. Chem. Phys.* **113** 7689
[12] Bates M A and Frenkel D 2000 Phase behavior of two-dimensional hard rod fluid *J. Chem. Phys.* **112** 10034
[13] Lagomarsino M C, Dogterom M and Dijkstra M 2003 Isotropic–nematic transition of long, thin, hard spherocylinders confined in a quasi-two-dimensional planar geometry *J. Chem. Phys.* **119** 3535
[14] Donev A, Burton J, Stillinger F and Torquato S 2006 Tetratic order in the phase behaviour of a hard-rectangle system *Phys. Rev.* B **73** 054109
[15] Vink R L C 2007 Liquid crystals in two dimensions: first-order phase transition and nonuniversal critical behaviour *Phys. Rev. Lett.* **98** 217801
[16] Martínez-Ratón Y 2007 Capillary ordering and layering transition in two-dimensional hard-rod fluids *Phys. Rev.* E **75** 051708
[17] Fortini A, Schmidt M and Dijkstra M 2006 Phase behavior and structure of model colloid–polymer mixtures confined between two parallel planar walls *Phys. Rev.* E **73** 051502
[18] Vink R L C, Binder K and Horbach J 2006 Critical behavior of a colloid–polymer mixture confined between walls *Phys. Rev.* E **73** 056118
[19] Vink R L C, De Virgiliis A, Horbach J and Binder K 2006 Phase diagram and structure of colloid–polymer mixtures confined between walls *Phys. Rev.* E **74** 031601
[20] De Virgiliis A, Vink R L C, Horbach J and Binder K 2007 Colloid–polymer mixtures between asymmetric walls: evidence for an interface localization transition *Europhys. Lett.* **77** 60002
[21] Fortini A, Bolhuis P G and Dijkstra M 2008 Effect of excluded volume interactions on the interfacial properties of colloid–polymer mixtures *J. Chem. Phys.* **128** 024904
[22] Oosawa F and Asakura S 1954 On interaction between two bodies immersed in a solution of macromolecules *J. Chem. Phys.* **22** 1255
[23] Vrij A 1976 Polymers at interfaces and the interactions in colloidal dispersions *Pure Appl. Chem.* **48** 471
[24] Virnau P and Müller M 2004 Calculation of free energy through successive umbrella sampling *J. Chem. Phys.* **120** 10925

[25] Landau D P and Binder K 2000 *A Guide to Monte Carlo Simulations in Statistical Physics* (Cambridge: Cambridge University Press)
[26] Binder K 1981 Finite size scaling analysis of Ising model block distribution functions *Z. Phys.* B **43** 119
[27] Low R J 2002 Measuring order and biaxiality *Eur. J. Phys.* **23** 111
[28] Dietrich S 1988 Wetting phenomena *Phase Transitions and Critical Phenomena* (London: Academic)
[29] Binder K and Hohenberg P C 1972 Phase transitions and static spin correlations in Ising models with free surfaces *Phys. Rev.* B **6** 3461
[30] Binder K and Hohenberg P C 1974 Surface effects on magnetic phase transitions *Phys. Rev.* B **9** 2194
[31] Diehl H W 1986 Field-theoretic approach to critical behaviour at surfaces *Phase Transitions and Critical Phenomena* (London: Academic)